

Entropic Elasticity of Double-Strand DNA Subject to Simple Spatial Constraints

C. Bouchiat

Laboratoire de Physique Theorique de l'Ecole Normale Supérieure
24, rue Lhomond, F-75231 Paris Cedex 05, France.

(Dated: March 22, 2024)

The aim of the present paper is the study of the entropic elasticity of the dsDNA molecule, having a crystallographic length L of the order of 10 to 30 persistence lengths A , when it is subject to spatial obstructions. We have not tried to obtain the single molecule partition function by solving a Schrodinger-like equation. We prefer to stay within a discretized version of the WLC model with an added one-monomer potential, simulating the spatial constraints. We derived directly from the discretized Boltzmann formula the transfer matrix connecting the partition functions relative to adjacent "effective monomers". We have plugged adequate Dirac δ -functions in the functional integral to ensure that the monomer coordinate and the tangent vector are independent variables. The partition function is, then, given by an iterative process which is both numerically efficient and physically transparent. As a test of our discretized approach, we have studied two configurations involving a dsDNA molecule confined between a pair of parallel plates. One molecule end is anchored to one plate by a biochemical bond. A stretching force F , normal to the plates, is pulling away the other end. In the first case, the crystallographic length L is smaller than the two-plate distance L_0 . The molecule feels, then, only the anchoring barrier effect. The predicted elongation-versus-force curve, is pushed upward with respect to the WLC model result. This effect is the most spectacular in the low force regime. For large forces say, $F_{\text{high}} = 5k_B T/A$, the elongation versus L is very well fitted by a straight line with a slope given by the standard WLC model and a constant term $\sim 1/2A$. In the second case, L takes values up to $L_{\text{max}} = 1.5L_0$. With a stretching force still equal to F_{high} , the standard WLC model predicts that the molecule cannot fit within the plates when $L > L_0 = 1.29L_0$. We have studied the evolution of the elongation derivative with respect to L , together with the mean square free-end fluctuations along the force. They both exhibit a sharp decrease when $L \rightarrow L_0$. We present a semi-quantitative argument suggesting that the terminal segment involving 20% of the internal monomers attains against the repulsive barrier when $L \rightarrow L_{\text{max}}$. In conclusion, we suggest extensions of the present work, relevant to the analysis of micromanipulation experiments. Finally, we have gathered into the Appendix formal developments, leading to a precise relation between the transfer matrix and the Hamiltonian methods for the study of spatially constrained dsDNA.

PACS numbers: 87.15.By, 61.41.+e

Introduction

In the last ten years Single Molecule Biophysics has become a very active field of research. Among the recently explored areas, one finds the observation, at the one-molecule level, of the biochemical interactions of the double strand DNA (dsDNA) with the various proteins involved in the duplication process (for two recent reviews see, for instance, the references [1, 2]). The protein-DNA interaction is detected by the observation, in real time, of the variations of the dsDNA elongation under the action of a fixed stretching force. It was clearly of interest to have a good physical understanding of the dsDNA elasticity measurements [3, 4, 5]. In absence of DNA supercoiling, this is provided by the so called "Worm Like Chain" (WLC) model [6, 7, 8] which gives a good description of the dsDNA entropic bending elasticity within a wide range of force, from few hundredths to few tens of piconewton.

In practice, the persistence length of a double helix is about five times the typical length resolution. It is, then, legitimate to use a rectifiable curve to represent the coarse-grained dsDNA chain. The basic hypothesis of the WLC model is to assume that the elastic-energy linear density is inversely proportional to the square of the chain-curvature radius. In the usual formulation of the WLC model, the relevant Statistical Mechanics variable is the tangent vector $\mathbf{t}(s) = d\mathbf{r}/ds$, where $\mathbf{r}(s)$ is the effective monomer coordinate and ds the rectifiable chain length element. The elastic molecular-chain energy, expressed in thermal unit $k_B T$, is given by the following line integral:

$$E_{\text{WLC}} = \int_0^L ds \frac{A}{2} \left(\frac{d\mathbf{t}(s)}{ds} \right)^2 - F \cdot \mathbf{t}(s); \quad (1)$$

where L is the crystallographic length of the polymer. A is the persistence length and $(d\mathbf{t}(s)/ds)^2$ is the inverse square of the curvature radius of the coarse-grained chain. $F = k_B T f$ stands for the stretching force, applied to the extremity of the chain. It follows from its very definition that \mathbf{t} is a unit vector. The partition function Z is given by

the functional Boltzmann integral:

$$Z = \int \mathcal{D}[\mathbf{r}] \mathcal{D}[\mathbf{t}] \exp(-E_{WLC}); \quad (2)$$

where the integration has to be performed over all the paths joining two points on the unit sphere. Exploiting the analogy with Feynman formulation of Quantum Mechanics (QM), the result of the functional integration is given in terms of the Hamiltonian operator [18]:

$$\hat{H}_{WLC} = -\frac{1}{2A} \nabla_t^2 - f \cdot \mathbf{t}; \quad (3)$$

where ∇_t^2 is the Laplacian on the unit sphere. In the limit where the $L \rightarrow A$, the elongation of the molecule under the action of a stretching force $F = k_B T f$ directed along the z axis is given by:

$$\langle z(L) \rangle = L \frac{\partial E_0(f)}{\partial f}; \quad (4)$$

where $E_0(f)$, the ground state eigen-energy of the Hamiltonian \hat{H}_{WLC} , can be obtained with a very good precision by solving numerically an ordinary differential equation with appropriate boundary conditions [8].

A. The problem of the Spatial Constraints in the WLC Model.

However, this approach becomes awkward if one wishes to impose physical constraints involving the monomer space coordinate. For instance, one may wish to confine the molecule within a certain region of space. This constraint can be formulated in terms of a potential, $V(r(s))$, acting on each monomer of coordinate $r(s)$. If the unitary tangent vector $\mathbf{t}(s)$ is the sole dynamical variable, one has to write $r(s) = \int_0^s \mathbf{t}(s^0) ds^0$ and the potential energy to be added to E_{WLC} has the non-local form:

$$E_{WLC}^{pot} = \int_0^{Z_L} ds \int_0^{Z_s} V(\mathbf{t}(s^0) ds^0); \quad (5)$$

This situation becomes worse if one studies self-avoiding effects described by a monomer-monomer repulsive potential, $V(r(s_1); r(s_2))$:

$$E_{WLC}^{SA} = \int_0^{Z_L} ds_1 \int_0^{Z_L} ds_2 V(\mathbf{t}(s_1^0) ds_1^0; \mathbf{t}(s_2^0) ds_2^0); \quad (6)$$

The obvious thing to avoid this problem for the monomer potential energy is to use the monomer coordinate $r(s)$ as a dynamical variable. It is convenient to consider a whole family of polymer models defined by the elastic-energy linear density:

$$E(s) = E_0(\kappa^2) + \frac{1}{2} A \kappa^2 - f \cdot \mathbf{r} + V(r); \quad (7)$$

where the WLC model can be recovered by an appropriate choice of $E_0(\kappa^2)$. But there is, clearly, a price to be paid: second-order derivatives appear now in the elastic-energy linear density, via the curvature term $\frac{1}{2} A \kappa^2$. The mapping onto an Euclidian Quantum Mechanics problem is no longer as evident as it was before.

B. A very brief review of previous studies on confined semi-flexible polymers.

Numerous authors have addressed themselves to the problem of finding an Hamiltonian describing semi-flexible polymers subjected to spatial constraints [12, 13, 14, 15, 16, 17, 18, 19, 20, 21, 22]. The basic idea was to formulate the problem in such a way that both the coordinate r and the "velocity" $\mathbf{v} = \dot{\mathbf{r}}$ appear as independent dynamical variables. Various mathematical techniques have been used to arrive to the Hamiltonian:

$$\hat{H} = \frac{1}{2A} \nabla_v^2 + E_0(v^2) + \mathbf{v} \cdot (\mathbf{r} - f) + V(r); \quad (8)$$

The case of the WLC model is obtained by choosing $E_0(v^2) / \frac{(v^2 - 1)^2}{2b^2}$ and going to the limit $b \rightarrow 0$. It leads to the spatially constrained WLC Hamiltonian:

$$\mathcal{H}_{\text{SCWLC}} = \mathcal{H}_{\text{WLC}} + \int_0^L dx V(x): \quad (9)$$

A group of authors [12, 13, 14, 15, 16, 17] have focused their analysis on the case of semiflexible polymers confined within a cylindrical tube having a radius much smaller than the persistence length. It corresponds to the choice $E_0(v^2) = 1$ with the running variable s being identified with the monomer-coordinate component along the axis of the tube. This can be viewed as the statistical physics analog of the Monge approximation for elastic rods. This model has been applied recently to interesting physical problems: the first one is the theoretical study of the flow of semiflexible polymers across cylindrical pores [16], a second one is the analysis of the unbinding transition between semiflexible polymers and directed polymers acting as one-dimensional attractive systems. [17].

The fully three-dimensional WLC Hamiltonian, involving both the coordinate r and the "velocity" $v = \dot{r}$, appears in references [18, 19, 20, 21, 22]. One of the most significant applications, which bears some resemblance with the work presented here, is found in reference [22], where the authors analyse a symmetric interface between two immiscible, semiflexible polymers.

C. Organization and Synopsis of the Paper

The aim of the present paper is the study of the spatial obstructions which are present in most micromanipulation experiments, involving a single dsDNA, immersed in a liquid thermal bath and possibly interacting with a single protein. These obstructive effects are expected to be significant in recent elongation experiments, involving molecular segments with a crystallographic length L of about ten persistence lengths [27].

We have not tried to obtain the partition function of a dsDNA molecule, subject to spatial constraints, by solving the partial differential equation associated with a Schrodinger-like problem, written with an imaginary time equal to β . In Section I, we rather stay within a discretized version of the WLC model involving N links (or effective monomers) of length $b = L/A$. The partition function Z_N is obtained by an iteration procedure involving the "transfer matrix" connecting adjacent monomers [24]. The "velocities" v_n , relative to the N effective monomers, are introduced in the discretized Boltzmann formula via appropriate Dirac δ -functions. The WLC model is obtained by choosing: $E_0(v_n^2) = b^2(2 - v_n^2)/2$ and by performing the integrals over the moduli $v_n = |\mathbf{j}_n|$ in the limit $b \rightarrow 0$, so that the tips of v_n are restricted to the unit sphere. After few manipulations, we arrive to a recurrence relation for the partition functions of molecules having their lengths L which increase by unit of b :

$$Z_{n+1}(\mathbf{r}_{n+1}; \mathbf{t}_{n+1}) = \exp(-\beta V(\mathbf{r}_{n+1})) \int d^3(\mathbf{t}_n) T_{\text{WLC}}(\mathbf{t}_{n+1}; \mathbf{j}_n) Z_n(\mathbf{r}_{n+1} - b\mathbf{t}_{n+1}; \mathbf{t}_n): \quad (10)$$

Here $T_{\text{WLC}}(\mathbf{t}_{n+1}; \mathbf{j}_n)$ is the transfer matrix relevant for the unconstrained WLC model. The above iteration procedure, which will be our basic tool for the study of the entropic elasticity of dsDNA subject to spatial constraints, exhibits a suggestive connection with a Markovian random walk in three dimensions.

The Section II is devoted to semirealistic applications of the above formalism. Our testing ground is the study of the entropic elasticity of a single dsDNA molecule confined between two parallel plates. One molecular end is anchored to one plate by a biochemical binding. A stretching force, normal to the plates, is pulling away the free molecular end from the anchoring plate. As long as we are mainly interested in the elongation of the dsDNA molecule, we can exploit the invariance under translations parallel to the plates and rotations around the stretching force to write a recurrence formula involving only longitudinal variables:

$$Z_{n+1}(z_{n+1}; \mathbf{t}_{n+1}) = \exp(-\beta V(z_{n+1})) \int_0^1 d(\cos \theta_n) T_{\text{WLC}}(\mathbf{t}_{n+1}; \mathbf{t}_n; \mathbf{f}) Z_n(z_{n+1} - b \cos \theta_{n+1}; \mathbf{t}_n);$$

where z and $\cos \theta$ are respectively the components along the force direction of the coordinate r and the unitary velocity vector \mathbf{t} .

For the sake of simplicity, we ignore, in this preliminary analysis, possible spatial obstructions associated with the stretching devices (magnetic and optical tweezers), but, in Section III, we suggest a practical way to take them into account. Two configurations are studied.

In the first one, the crystallographic length L is supposed to be shorter than the two-plate distance L_0 , so that the entropic elasticity is affected only by the anchoring plate barrier. For a relatively short molecule ($L/A = 12$), we compute the elongation-versus-force curve, which is expected to be pushed upward with respect to the unconstrained WLC model predictions, notably for the zero-force case. In the case of relatively high force F , i.e. $\beta F A = (k_B T) = 5$,

the elongation $h(z(L))$ versus L is very well fitted, within the interval $2A \leq L \leq 10A$, by a straight line with a slope = 0.771 and a constant term = $1.22A$. The slope turns out to be very close to the value predicted by the unconstrained WLC model in the limit $A \ll L$, namely, 0.775. If the second plate is pushed further away, the predictions of the two models for $h(z(L))$ will coincide when $A \ll L$ up to a 0.5% correction, which could be due to our use of a discretized version of the WLC model.

In the second configuration, L is allowed to take values up to $1.5L_0$, with the same stretching force value as above: $F_A = (k_B T) = 5$. A molecule, elongated according to the unconstrained WLC model cannot fit within the plates when its crystallographic length L is larger than the critical value $L_c = 1.29L_0$, associated with the elongation $h(z(L)) = L_0$. We have studied the evolution of the terminal monomer statistics when L varies within the interval: $0.6L_0 \leq L \leq 1.5L_0$, using as representative quantities the elongation derivative $dh(z(L))/dL$ and the mean square of the free-end fluctuations along the stretching force direction, i.e. $\langle z^2(L) \rangle = \langle h(z(L)) - h(z(L)) \rangle^2$. When $L \leq L_0$ these two quantities follow rather closely the predictions of the unconstrained WLC model but they both start a rather sharp decrease when $L > L_0$. The elongation $h(z(L))$ is no longer an extensive physical quantity and goes slowly to L_0 . As to the fluctuations $\langle z^2(L) \rangle$, they are reduced by a factor 10 with respect to the unconstrained WLC model prediction.

In the case $L = L_{max} = 1.5L_0$, we give a semi-quantitative analysis of the internal monomers statistics, when the monomer number varies within the interval $L_{min} < n < L_{max}$. The characteristic feature of our model lies in the fact that all the monomers are confined between the two plates. We call this type of spatial constraint an internal confinement (IC) in contrast with the external confinement (EC) describing a situation where the confining $V(z)$ is acting only upon the terminal monomer. A rather good physical understanding of what is going on near the repulsive barrier has been obtained within a Gaussian model, supplemented by a square-well potential with a depth $k_B T$. Choosing a configuration with the same value of L as before, we find, without too much surprise, that in the IC model the terminal segment involving 20% of the internal monomers attains against the repulsive barrier, while in the EC model all the monomers, except the terminal one, can move rather freely across the repulsive barrier.

In Section III, we suggest possible applications or extensions of the work presented in the present paper; let us mention the two of them which concern directly the micro-manipulation experiments:

We propose a simple procedure involving a two-plate confinement model which may lead to an estimate of the spatial obstruction effects associated with the magnetic tweezer.

It is relatively straightforward to generalize the spatially constrained WLC model, within its transfer matrix formulation, to the RLC model [9, 10, 11], which incorporates both bending and twisting rigidities. The anchoring barrier effects are expected to be significant when the reduced supercoiling parameter is above the threshold - at fixed force - for the creation of plectonem configurations. The stretching potential energy vanishes for such structures, allowing them to wander irrespective of the sign of twist.

The Appendix is devoted to a comparison of two possible approaches to the elastic entropy elasticity of dsDNA subject to spatial constraints. The first one, used in the present paper, is the transfer matrix method which leads to an iterative construction of the partition function, within a discretized version of the constrained WLC model. The second approach [12, 13, 14, 15, 16, 17, 18, 19, 20, 21, 22] is based upon the solution of a Schrodinger-like equation, written with an imaginary time variable τ involving the Hamiltonian given by eq. (9). To achieve our purpose, we have found convenient to use the auxiliary variable method in order to eliminate the second order derivative in the elastic energy density given by eq. (12). It is, then, a rather straightforward affair to obtain the transfer operator $\hat{\mathcal{P}}$ - associated with the transfer matrix-, from which one derives the Hamiltonian $\hat{\mathcal{H}}$ by taking the continuous limit $b \rightarrow 0$. Making use of the leeway inherent to any discretization procedure, one can obtain a symmetric version of $\hat{\mathcal{P}}$, which coincides with the exact evolution operator $\exp(-b\hat{\mathcal{H}})$, up to corrections of the order of b^3 .

It is not too difficult to elucidate the physical interpretation of the auxiliary variable u : we have proved that the conjugate momentum p_u appearing in $\hat{\mathcal{H}}$ is just the "velocity" v . Performing an appropriate change of basis, one obtains immediately an expression of $\hat{\mathcal{H}}$, identical to the r.h.s. of eq.(8). With the proper choice of $E_0(\tau^2)$, one then arrives to the spatially constrained WLC Hamiltonian, $\hat{\mathcal{H}}_{SCWLC}$, given by eq.(9) [12, 13, 14, 15, 16, 17, 18, 19, 20, 21, 22]. Finally, as an internal check, we derive a symmetric transfer matrix from the transfer operator $\hat{\mathcal{P}}$, associated with the Hamiltonian $\hat{\mathcal{H}}_{SCWLC}$. By making suitable approximations, we recover the transfer matrix, physically more transparent, which is derived directly from the Boltzmann formula in Section I.

I. A TRANSFER MATRIX APPROACH TO STRETCHED DS-DNA SUBJECT TO SPATIAL CONSTRAINTS

We wish, first, to consider the statistical properties of a class of polymer models described by the linear elastic-energy density $E(s)$ depending upon the monomer coordinate $r(s)$, together with its first and second order derivatives, $\underline{r} = \frac{dr}{ds}$ and $r = \frac{d^2}{ds^2}(r)$. The variable s with $0 \leq s \leq L$ results from a coarse graining of the molecular chain, having a crystallographic length L . Note that s does not coincide necessarily with the arc-length s of a rectifiable curve.

The partition function for fixed free-end polymers is given by a functional integral involving the standard Boltzmann statistical weights :

$$Z = \int \mathcal{D}[\underline{r}] \exp \int_0^L E(s) ds ; \quad (11)$$

$$E(s) = E_0(\underline{r}^2) + \frac{1}{2} A r^2 - \underline{r} \cdot \underline{V}(r) ; \quad (12)$$

where the functional integration goes over all the paths joining the free ends of the chain of fixed coordinates $r(0)$ and $r(L)$.

We stress that, here, the potential $V(r)$, simulating the spatial constraints, is clearly acting upon all the monomers of the molecular chain, contrary to confining models where the potential $V(r)$ is acting, only, upon the terminal monomer, e.g. via an attached bead. In this latter case, constraints can be trivially implemented by adding in the elastic density (12) the "velocity" dependent contribution $\underline{r} \cdot \underline{V}(r)$.

To compute the partition function we have to resort to a discretization of the variable s : $s_n = nb$. The molecular chain is then represented by N elementary links or effective monomers with $N = L/b$. Assuming that the effective monomer length b is much smaller than the persistence length A , we can write:

$$\underline{r}_n = \frac{r_n - r_{n-1}}{b} ; \quad r_n = \frac{r_n - 2r_{n-1} + r_{n-2}}{b^2} ; \quad (13)$$

It is then convenient to introduce the discretized form of the elastic-energy density $E_{disc}(n)$ obtained by plugging the formulas (13) into the right hand side (r.h.s.) of equation (12):

$$E_{disc}(n) = E_0 \left(\frac{r_n - r_{n-1}}{b} \right)^2 + \frac{1}{2} A \left(\frac{r_n - 2r_{n-1} + r_{n-2}}{b^2} \right)^2 - \underline{r}_n \cdot \left(\frac{r_n - r_{n-1}}{b} \right) + V(r_n) ; \quad (14)$$

The partition function is then given as an integral of a product of $N-1$ monomer-coordinate- \underline{r}_n functions:

$$Z = \int \prod_{n=1}^{N-1} d^3 r_n \int \prod_{n=2}^N d^3 \underline{r}_n \exp \left(-b E_{disc}(n) \right) g_{in}(r_1; r_0) ; \quad (15)$$

where the monomers coordinates r_0 and r_N are kept fixed. The starting partition function is taken to be :

$$g_{in}(r_1; r_0) = \exp \left(-b E_0 \left(\frac{r_1 - r_0}{b} \right)^2 - b V(r_1) \right) ; \quad (16)$$

From the above expression of the partition function one could write down easily a transfer matrix connecting the probability distributions relative to pairs of adjacent monomers:

$$Z_{n+1}(r_{n+1}; r_n) = \int d^3 r_{n-1} \int d^3 r_{n-2} \exp \left(-b E_{disc}(n+1) - b E_{disc}(n) \right) Z_{n-1}(r_{n-1}; r_{n-2}) ; \quad (17)$$

This approach turns out to be rather awkward in the particular case of the WLC model but may be useful for other models. The standard trick is to introduce the "velocities" $\underline{v}_n = \underline{r}_n = (r_n - r_{n-1})/b$ as new variables in the discretized functional integral (15) via the trivial identity:

$$1 = \int d^3 \underline{v}_n \delta \left(\underline{v}_n - \frac{r_n - r_{n-1}}{b} \right) ;$$

Making some obvious manipulations, one gets a new expression for the partition function as an integral over paths joining two elements in the 6-dimension space obtained by taking the direct sum of the coordinate r and velocity \underline{v}

spaces:

$$Z_N(r_N; v_N) = \int_{n=1}^{N-1} d^3 r_n d^3 v_n f^{(N)}(v_n, \frac{r_n - r_{n-1}}{b}) \exp[-b E_0(v_n^2) + \frac{1}{2} A (\frac{v_n - v_{n-1}}{b})^2] f_{n-1} v + V(r_n) g Z_1(r_1; v_1): \quad (18)$$

For practical reasons, the coordinate r_0 will be assumed from now on to be a random variable with the probability distribution $P(r_0)$. Then, $Z_1(r_1; v_1)$ is given by:

$$Z_1(r_1; v_1) = \exp[-b E_0(v_1^2)] f_{-1} v + V(r_1) P_0(r_1 - b v_1): \quad (19)$$

If one performs explicitly the integration upon the v_n variables in the r.h.s of equation (18), one readily recovers the r.h.s of equation (15) with $Z_{in}(r_1; r_0)$ replaced by its average over r_0 . Only nearest-neighbour monomers with given coordinate and velocity are now connected. It is then possible to write down a recurrence relation between adjacent intermediate partition functions $Z_n(r_n; v_n)$ relative to chains having a crystallographic length $s_n = bn$:

$$Z_{n+1}(r_{n+1}; v_{n+1}) = \int d^3 r_n d^3 v_n T(r_{n+1}; v_{n+1} | r_n; v_n) Z_n(r_n; v_n): \quad (20)$$

The transfer matrix $T(r_{n+1}; v_{n+1} | r_n; v_n)$ is easily read off from the r.h.s of equation (18):

$$T(r_{n+1}; v_{n+1} | r_n; v_n) = f^{(N)}(v_{n+1}, \frac{r_{n+1} - r_n}{b}) \exp[-b(V(r_{n+1}))] \exp[-b E_0(v_{n+1}^2) + \frac{1}{2} A (\frac{v_{n+1} - v_n}{b})^2] f_{n-1} v_1: \quad (21)$$

Performing the integration upon r_n , we arrive to the final form of the recurrence relation:

$$Z_{n+1}(r_{n+1}; v_{n+1}) = \int d^3 v_n \exp[-b E_0(v_{n+1}^2) + V(r_{n+1})] d^3 v_n \exp[\frac{1}{2b} A (v_{n+1} - v_n)^2] f_{n-1} v_1 Z_n(r_{n+1} - b v_{n+1}; v_n): \quad (22)$$

In order to apply the above formula to the WLC model with spatial constraints, we have to choose an adequate form for the function $E_0(v^2)$. The solution is rather simple: one introduces the small length b such that $b \ll 1$ and one takes for $E_0(v^2)$ the following expression:

$$E_0(v_n^2) = b \frac{(v_n^2 - 1)^2}{2 b^2}: \quad (23)$$

Indeed, with this choice, we write the volume element in the velocity space as: $\int d^3 v_n = \int_{-R}^R v_n^2 dv_n d^2(t_n)$, where $d^2(t_n)$ is the infinitesimal solid angle around the unit vector t_n taken along v_n , written as $v_n t_n$. Then, in the limit $b \ll 1$, $\exp[-b E_0(v_n^2)]$ reduces, up to a numerical constant, to the δ -function: $\delta(v_n - 1)$. As a consequence, integrating over v_n within the same limit, leads to an expression of the r.h.s of equation (18) readily obtained by making the replacement:

$$d^3 v_n \rightarrow d^2(t_n); \quad v_n \rightarrow t_n:$$

The transfer matrix describing stretched dsDNA within the WLC model with spatial constraints is then simply obtained from eq.(22) using the same replacement rules:

$$Z_{n+1}(r_{n+1}; t_{n+1}) = \int d^2(t_n) \exp[-b(V(r_{n+1}))] d^2(t_n) \exp[\frac{A}{2} (t_{n+1} - t_n)^2] f_{n-1}(t_{n+1} + t_n) Z_n(r_{n+1} - b t_{n+1}; t_n): \quad (24)$$

To make easier the comparison with the standard WLC model, we have replaced in the above equation $f_{n-1}(t_{n+1} + t_n)$ by $f_{n-1}(t_{n+1} + t_n) = 2$. Such a modification amounts to the replacement of a rectangular discretized integration by a

trapezoidal one. What appears now in the r.h.s of the recurrence relation is the transfer matrix relative to the standard WLC model:

$$T_{WLC}(t_{n+1}; t_n) = \exp \left[\frac{A(t_{n+1} - t_n)^2}{2b} + \frac{b}{2} f(t_{n+1} + t_n) \right] : \quad (25)$$

In the Appendix, we are going to show, within a more general context, that $T_{WLC}(t_{n+1}; t_n)$ coincides, up to corrections of the order of $(b/A)^3$, with the exact transfer operator $\exp \left[\frac{b}{2A} \mathcal{H}_{WLC}^2 \right] f(t)$.

We are, now, ready to give the partition-function recurrence relation which will be our basic tool for the study of the entropic elasticity of dsDNA subject to spatial constraints:

$$Z_{n+1}(r_{n+1}; t_{n+1}) = \exp \left(-bV(r_{n+1}) \right) \int dt_n T_{WLC}(t_{n+1}; t_n) Z_n(r_{n+1} - bt_{n+1}; t_n) : \quad (26)$$

The iterative construction of the partition function $Z_n(r_n; t_n)$ has a transparent physical meaning. Indeed, it has a suggestive interpretation in terms of a Markovian random walk model in three dimensions: the $(n+1)^{th}$ step is given by bt_{n+1} ; its length is b and its direction, defined by the unitary vector t_{n+1} , is correlated to that of the previous step t_n through the correlation function $C(t_{n+1}; t_n) / T_{WLC}(t_{n+1}; t_n)$. Within our unit conventions, the "potential" $V(r)$ stands for a potential energy by unit molecular length, written in thermal units, so that $bV(r_{n+1}) = k_B T bV(r_{n+1})$ represents the amount of energy to be exchanged with the thermal bath by performing the $(n+1)^{th}$ step. The exponential in front of the r.h.s of equation (26) is just the associated Boltzmann factor.

II. THE STRETCHING OF A DS-DNA MOLECULE CONFINED BETWEEN TWO PARALLEL PLATES.

In this section, we apply our iterative version eq.(26) of the spatially constrained WLC model to the confinement of a single dsDNA molecule between two parallel plates – called hereafter Plate 1 and Plate 2 – separated by a distance L_0 . One molecular end is anchored upon Plate 1. The other end is attached, for instance, to a magnetic bead pulled by a magnetic tweezer. We do not pretend, here, to describe a fully realistic situation since, for the sake of simplicity, we ignore the spatial constraints associated with the finite dimensions of the magnetic bead. In Section III of this paper, we shall suggest a self-consistent procedure, within the two-plate model, which will lead to an estimate of the bead obstruction effect. The stretching force is assumed to be normal to the two plates and is pulling away the molecular end from the anchoring plate. The dimensions of the plates normal to the force, measured from the anchoring point, are assumed to be much larger than L_0 and will be considered as infinite. Two physical configurations have been considered:

1. L_0 is supposed to be larger than the crystallographic length L . (In our explicit computations we have taken $L_0 = 40 \text{ \AA}$ and $L = 12 \text{ \AA}$.) It means that even for large stretching forces the molecular end stays far away from Plate 2. This will allow us to study the deviations of the elongation from the WLC model prediction due to the presence of the anchoring plate (Plate 1), provided we ignore the spatial obstruction of the pulling device.
2. The crystallographic length L is larger than L_0 so that, for large forces, the fully stretched molecule does not fit inside the plates. We have studied, within the WLC model, how the molecule adapts itself to a confined situation where the elongation predicted by the unconstrained WLC Model reaches values significantly larger than L_0 .

A. Basic formulae for the two-plate confinement configurations.

Our confinement configurations, defined by the two confining plates and the stretching force, are invariant, first, under rotations around the z -axis defined by the anchoring point and the stretching force direction, second, under the translations within the x,y plane. We shall consider a molecular ensemble where the anchoring monomer is uniformly distributed over the x,y plane. The iteration procedure can then be organized in such a way that at each step the partition function $Z_n(r_n; t_n)$ depends only upon the two independent variables: z_n and $\cos \theta_n$, which are respectively the components upon the z -axis of the monomer coordinate r_n and the tangent vector t_n . If this condition is satisfied at the step n , $Z_{n+1}(z_{n+1}; \cos \theta_{n+1})$ is then easily obtained from an azimuthal average around the z -axis of the two sides of eq.(26):

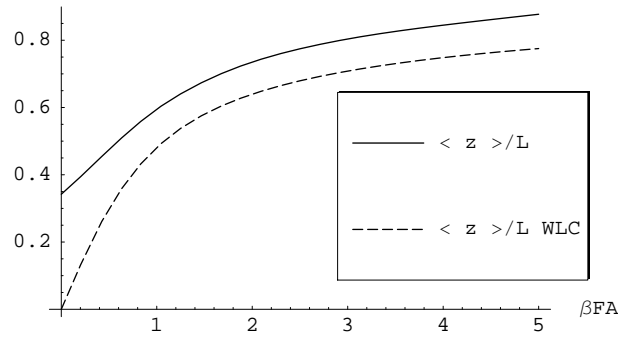


FIG. 2: Illustration of the effects of the anchoring plate barrier upon the elongation-versus-force curve. The upper curve (full line) gives the prediction of the spatially-constrained WLC model when $L=A=12$. The other plate is lying at a distance $L_0 = 10L=3$ and, as a consequence, has no effect upon the elongation. The fact that the elongation curve is pushed upward with respect to the unconstrained WLC prediction (dotted curve) has a simple qualitative explanation: because of the anchoring plate barrier the $z < 0$ half space is not accessible to the nucleotides, whatever the stretching force.

A look at the potential $V(z)$ on Fig. 1 shows that z_0 can take negative as well as positive values within the range $(-A; A)$, so that a centered Gaussian curve looks quite realistic if $A \gg L$. Similarly the tangent-vector z -axis projection, $\cos \theta_0$, lies within the interval $(-1; 1)$, so that a $\cos \theta_0$ uniform distribution seems to be an acceptable guess. We note, finally, that our choice of $Z_0(z_0; \theta_0)$ satisfies the smoothness condition assumed in the previous section. The $n=1$ partition function $Z_1(z_1; \theta_1)$ is then readily obtained by plugging $Z_0(z_0; \theta_0)$ in the r.h.s. of the recurrence relation (27).

We would like to give, now, a few indications about the numerical methods we have used to run the transfer matrix iteration process.

In order to perform the integral over z_n , we use the following discretization procedure. We divide the variation interval $0 \leq z_n \leq L$ into n_s segments $\frac{(s-1)L}{n_s} \leq z_n < \frac{sL}{n_s}$. The integral over each segment is done with the standard Gaussian method involving n_g abscissae and n_g attached weights. The integral over the full z_n interval is then approximately given by a discrete weighted sum over $d = n_s n_g$ points:

$$\int_0^L f(z_n) \sin \theta_n dz_n = \sum_{i=1}^{X^d} w_i \sin \theta_i f(z_i):$$

The transfer matrix iteration involves a z variable translation $z_n \rightarrow z_{n+1} = z_n + b \cos \theta_{n+1}$ to be performed upon $Z_n(z_n; \theta_n)$ for each value $n = 1, \dots, N$. This is achieved by building at each step the interpolating function $Z_{n;int}(z; \theta_i)$ associated with the array: $fz_1 = z_{min} + lb; Z_n(z_1; \theta_i)g$ with $1 \leq i \leq n_{max}$. An appropriate choice of n_{max} leads to a physically relevant sample of the monomer coordinates throughout the iteration process.

For more extensive computations than those presented in this paper, one should consider a potentially more efficient method involving the Fast Fourier Transform (FFT) algorithm. It is based upon the remark that a variable translation performed upon a given function reduces to a phase shift upon its Fourier transform: $\mathcal{F}(p; \theta_i) \rightarrow \exp(-ib \cos \theta_i) \mathcal{F}(p; \theta_i)$. An inverse FFT will then be required to perform the multiplication by the Boltzmann factor.

B. Modification of the elongation-versus-force curve induced by the anchoring plate barrier.

We would like to present, here, the results of a numerical simulation based upon the iteration process built up from the recurrence relation given in eq.(27). Our aim was to study the barrier effect of the anchoring plate (Plate 1.) upon the elongation-versus-force curve. This corresponds to the configuration 1, introduced previously, where the distance between the plates L_0 is larger than the crystallographic length L . The values used in our simulation are $L_0 = 40 \text{ \AA}$ and $L = 12 \text{ \AA}$. It is, then, clear that Plate-2 plays no role since we have decided to ignore the eventual presence of a magnetic bead attached to the molecule free end. At each step n we store the normalized z_n -probability distribution, $P_n(z_n; \theta_n)$, where $\beta = F/A = (k_B T)^{-1}$ is the reduced force parameter. We have plotted in Figure 2 the relative molecular elongation $\langle z \rangle / L$ versus βFA , where $N = L/b$. The dotted curve represents the prediction of the standard WLC model which assumes that the anchoring device reduces to a point.

The full curve corresponds to the elongation-versus-force obtained in our simulation within a spatially constrained WLC model; it exhibits clearly the anchoring-plate barrier effect which leads to a relative elongation of 34% in the zero

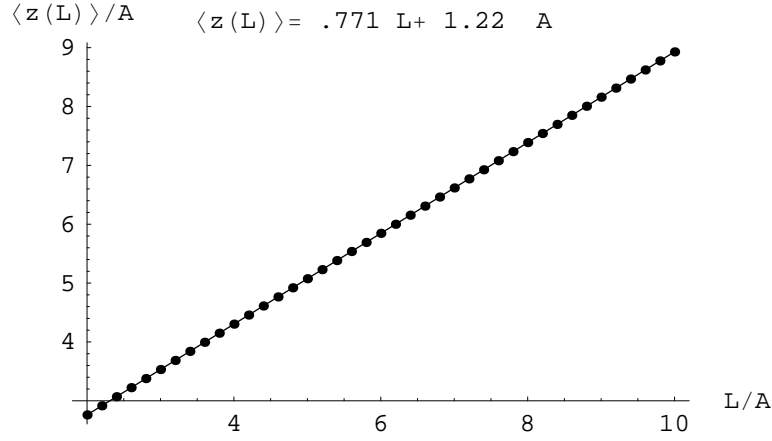


FIG. 3: Linear fit to a set of $\langle z(L) \rangle$ values, coming out from our iteration procedure in the case $\beta = 5$, when L increases from $2A$ to $10A$. The slope given by the fit, 0.771 is in good agreement with the prediction of the standard WLC model, 0.775 , valid in the limit $A = L \rightarrow 1$.

force limit. For higher forces, the two curves become approximately parallel with an offset of about 10%. It is possible to get from our simulation an expansion in powers of A/L at fixed force, giving the upward elongation displacement $\bar{h}_z = Li$ induced by the anchoring plate barrier. As an illustration, we give the result for two typical forces corresponding to $\beta = 0$ and $\beta = 1$. We found that the second-order expansion, $\bar{h}_z = Li = a_1(\beta) \frac{A}{L} + a_2(\beta) \frac{A^2}{L^2}$, gives a very good fit to our simulation data within the range: $5A \leq L \leq 30A$. For $\beta = 0$ we get: $a_1(0) = 1.00$; $a_2(0) = 0.65$. The large value of $a_1(0)$ can be interpreted in terms of an hemispheric molecular cluster around the anchoring point with a radius growing like \sqrt{N} . The results look rather different when $\beta = 1$: $a_1(1) = 0.06$; $a_2(1) = 1.57$. The strong decrease of the $\frac{A}{L}$ coefficient - combined by the $\beta = 2$ results - seems to suggest that the anchoring plate barrier affects only a dsDNA segment having a fixed length A when $\beta \rightarrow 1$.

When one looks at the curves of Fig 2, one may wonder if they are going to meet in the limit of high force, as they should, since $\bar{h}_z(L)i=L$ goes to one for the two cases. Before trying to push the present computation to larger values of β , one has to keep in mind two things, one, the dotted curve corresponds to the limit $A=L \rightarrow 1$ while we are working with $A=L \rightarrow 0.1$, second, the dotted curve goes rather slowly to the limit $\beta \rightarrow 1$: indeed, $\bar{h}_z(L)i=L = 0.95$ for $\beta = 100$. Our computation will simply not work under these two extreme conditions. There is fortunately another way to make a meaningful comparison of the two models: it is to look at the derivatives $\frac{d\bar{h}_z(L)i}{dL}$ instead of $\bar{h}_z(L)i=L$. In the unconstrained WLC model computations these two quantities are identical but this is not in general true in presence of spatial constraints. We have plotted in Fig. 3 the values $\bar{h}_z(L)i$ obtained by our iteration procedure in the case $\beta = 5$. The results correspond to the big dots and cover the range of L values: $2A \leq L \leq 10A$. We have performed a linear fit to the data, $\bar{h}_z(L)i_{fit} = 0.771L + 1.22A$, which, as it is apparent on Fig. 3, works beautifully. The fitted slope, 0.771 , is very close to that given by the unconstrained WLC model, namely, 0.775 . We also note that the constant term $1.22A$ has the same order of magnitude as the one obtained previously for $\beta = 1$: This strongly suggests that, if the Plate-2 is pushed to infinity, the two models will give identical predictions, for the elongation $\bar{h}_z(L)i=L$ in the limit $A \rightarrow L$. We have ignored the 0.5% difference, which may be attributed to our use of a discretized model with $b=A = 0.1$.

C. Statistical behaviour of stretched molecules having cristallographic lengths larger than the two-plate distance.

This section is devoted to the analysis of the results of the transfer-matrix iteration for molecular chains having cristallographic lengths within the interval $20A \leq L \leq 30A$ when they are confined between two plates separated by a distance $L_0 = 20A$. The stretching force is specified by taking the value $\beta = F A / (k_B T) = 5$ for the reduced force parameter. The unconstrained WLC model would lead to a relative elongation $\bar{h}_z(L)i=L = 0.775$, to be compared with the ratio $L_0/L = 2/3 \approx 0.667$. As a consequence, molecules having a cristallographic length $L > L_c = L_0/0.775 = 1.29L_0 = 25.8A$, could not fit within the two plates if stretched according to the WLC model prediction.

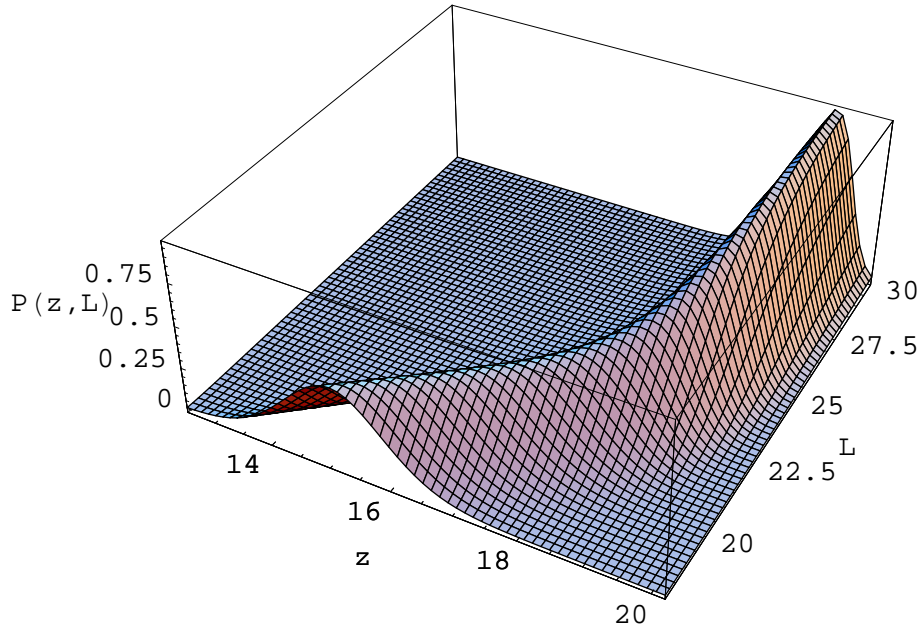


FIG. 4: 3-D plot illustrating the probability distribution of the coordinate z of the molecular end, $P(z;L)$, when the crystallographic length L varies from $0.9L_0$ to $1.5L_0$ with $L_0 = 20$ Å. In our iterative computation, we have taken a stretching force such that the elongation predicted by the unconstrained WLC model is $h(z;L) = 1.16L_0$ when L takes its maximum value. It is then clear that such a molecule, stretched according to the usual WLC model, could not fit between the plates. When L approaches its maximum value $1.5L_0$, the elongation $h(z;L)$ is no longer increasing like L but tends to its maximum possible value L_0 ; at the same time the slope of the hill exhibited by $P(z;L)$ is becoming steeper. This indicates a decrease of the longitudinal fluctuations of the terminal monomer.

1. The terminal monomer statistics.

Our iteration procedure provides us with the terminal monomer distributions $P(z;L)$ for various molecular lengths $L \leq 30$ Å. At each step we store the probability $P_n(z(n))$ and by identifying $L = n b$ we build the discrete set: $P(z;nb) = P_n(z)$. The probability distribution $P(z;L)$ is then obtained by interpolation. We have displayed in Fig. 4 a 3-D plot of $P(z;L)$. It allows us to follow in a continuous way how the DNA molecule manages to satisfy the two-plate space constraints. When $18 \leq L \leq 20$ the molecule does not feel yet the Plate-2 barrier and the hill ridge, projected upon the $(z;L)$ plane, follows a straight line with a slope $z = N$ given by the standard WLC model. When L enters the domain $20 \leq L \leq 30$ the ridge bends under the barrier repulsion to become parallel to the plates. At the same time the hill slope becomes steeper under the combined effects of the stretching force and the confining plates.

In Fig 5 we present the results of a quantitative analysis of the terminal monomer statistics described previously in a qualitative way. The solid line curve gives the derivative of the chain elongation $\frac{dh(z;L)}{dL}$ as a function of L . When L stays within the interval $12 \text{ Å} \leq L \leq 20 \text{ Å}$, the rate of variation per unit length $h(z;L)$ stays constant as in the unconstrained WLC model: the elongation still behaves as an extensive quantity. We have verified that the height of the plateau agrees within a few tenths of a percent with the exact WLC prediction quoted above. When the crystallographic length of the molecular chain is going gradually from $L_0 = 20$ Å to $L = L_{\max} = 30$ Å, the elongation derivative with respect to L starts a rather sharp decrease towards 0. The elongation $h(z;L)$ is no longer extensive and goes slowly to $1.9 \text{ Å} \times L_0$: The dotted line of Fig 5 gives, as a function of L , the mean square free-end fluctuations along the stretching force direction $\langle z^2(L) \rangle = \langle h(z(L)) - h(z(L)) \rangle^2$. If $L \leq L_0$, then, $\langle z^2(L) \rangle$ increases linearly with L and the slope stays very close to that predicted by the WLC model. When L varies from L_0 to L_{\max} , $\langle z^2(L) \rangle$ undergoes a sharp decrease and reaches a minimal value ten times below the prediction of the unconstrained WLC model.

We would like to stress that a basic physical feature of our model is the Internal Confinement (IC), which simply means that all the monomers are constrained practically to stay within the space domain: $0 \leq z \leq L_0$. We will find helpful, later on, to consider also models involving an External Confinement (EC): the confining potential $V(r)$ is acting only upon the terminal monomer, for instance via an attached bead, so that the internal monomers are no longer spatially constrained. This type of confinement can be implemented by adding to the elastic density (12) the velocity dependent contribution $\frac{1}{2} \dot{r}^2 V(r)$. We have calculated $\frac{dh(z;L)}{dL}$ and $\langle z^2(L) \rangle$ versus L using the EC version of

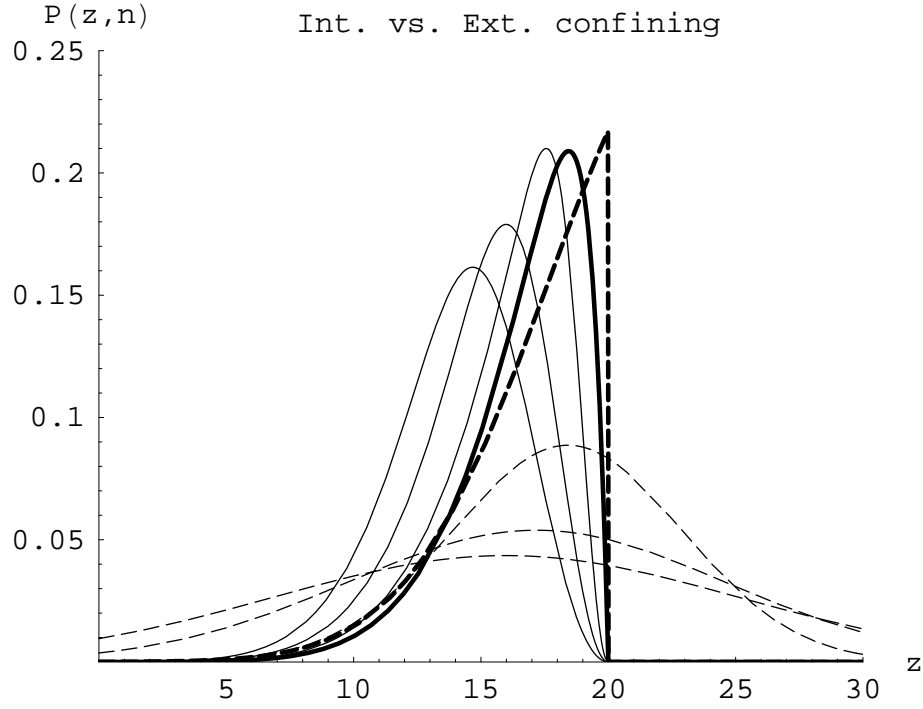


FIG. 6: Differences between the internal monomer statistics depending upon the type of the Gaussian confining model. In the internal-confining (IC) model, all the monomers feel the confining potential. This contrasts with the external-confining (EC) model where the confining plate, at $L_0 = 20a$, is acting only upon the terminal monomer. The solid and dashed curves stand respectively for the IC and EC probability distributions $P(z; n)$ for $L_{int} = nb = 25a; 27a; 29a$, in that order from left to right; the thick lines are relative to the terminal monomer. The attenuating of the terminal segment – 20% of the monomers – against the repulsive barrier is conspicuous in the IC model while nothing similar is visible in the EC case, where internal monomers are allowed to wander beyond the plate.

On the other hand, the formula giving $P_{EC}(n; z_n)$ is obtained by performing in the r.h.s. of the above equation the following replacements:

$$f_{z_N} \rightarrow f_{z_1} \rightarrow bV(z_1); \quad \hat{H}_z \rightarrow \hat{H}_{z_0}:$$

The QM problems associated with both \hat{H}_{z_0} and \hat{H}_z can be easily solved analytically by taking for $V(z)$ a square well with a depth $k_B T$. The results displayed in Fig. 6 have been obtained with model parameters leading to basic physical quantities as close as possible to those appearing in the previous WLC analysis: $L_{max} = nb = 30a$; $L_{int} = nb = 25a; 27a; 29a$; $L_0 = 2 = 3L_{max} = 20a$; $af = 0.775$. This last condition leads to $hz(L) = L = 0.775$ in absence of confinement.

In Fig. 6 the solid and dashed curves refer respectively to the IC and EC model. The two thick lines are relative to the terminal monomer distributions. The z -probability distributions for internal monomers with $L_{int} = 25a; 27a; 29a$ – appearing in that order from left to right on Fig. 6 – exhibit very striking differences between the IC and the EC model. The IC curves suggest that the terminal chain-segment, involving 20% of the internal monomers, is subject to a progressive attenuating against the repulsive barrier. In contrast no such effect is observed with the EC curves: the EC internal monomers wander rather freely across the repulsive barrier while the terminal monomer is practically stuck to it, as it should.

III. PERSPECTIVES AND POSSIBLE EXTENSIONS.

We would like to suggest some possible applications or extensions of the work presented in this paper.

The transverse fluctuations of a single dsDNA molecule attached at both extremities to a plane surface have been observed recently [26]. The experimental data have been analysed with success by a dynamical model derived from the WLC model, ignoring the barrier effect of the surface. We believe it is of interest to understand this remarkable result within the spatially constrained WLC model, using a closely related conformation, more easily

to handle than the actual one. Only one extremity of dsDNA segment is assumed to be anchored to the surface while a pulling force parallel to the surface is acting upon the free end. The Boltzmann factor associated with the surface barrier effect will be described by the rounded-off step function introduced in Section II.

The dsDNA configurations studied in Section II were not fully realistic since we have ignored the spatial obstruction coming from the magnetic (or optical) tweezers. In practice the dsDNA is attached near the bottom of the spherical bead. In recent micro-manipulation experiments [27] the tendency is to use relatively short dsDNA segments with 2000 base pairs, corresponding to $L = 680 \text{ nm}$. For a stretching force $F = 0.3 \text{ pN}$, the molecule explores the surface around its anchoring point over a distance of the order of the root mean square transverse fluctuation: $\langle x^2 \rangle = \hbar z / (k_B T) = F^{-1/2} \cdot 1.55 \text{ \AA} = 85 \text{ nm}$, which is about ten times smaller than the bead diameter. The DNA molecule does not really feel the curvature of the bead surface; therefore the bead can be approximated by its tangent plane. Ignoring the longitudinal fluctuations, we substitute to the obstructive bead a plane barrier lying at a distance $l = \hbar z$ from the anchoring plate. To compute the bead obstruction correction, we suggest to follow a method similar to that used in Section II, but with one difference: instead of computing the elongation in terms of the pulling force, we shall rather get the force as a function of the elongation. Let F_0 be the force associated with the given elongation $l = \hbar z$, when one ignores the bead obstruction. The next step will be to compute the elongation in presence of the plate, substitute for the bead, starting from a pulling force $F < F_0$ and letting it grow until it reaches the value F_1 where the elongation is back to its initial value l . The bead obstruction correction to the force associated with a given elongation l will then be estimated as $F = F_1 - F_0$. An improvement of the precision of the computations, with respect to that obtained in Section II, will be necessary. This can be achieved by taking a smaller link length b , say $b = A/30$.

In references [9, 10, 11] the WLC model has been generalized to a Rod Like Chain (RLC) Model, involving both bending and twisting rigidities. This makes possible the study of supercoiled dsDNA entropic elasticity below the denaturation threshold. One can readily modify the RLC model in order to incorporate spatial constraints. The recurrence relation for the partition function $Z_n(z_n; n; \cdot)$ relative to a supercoiled DNA molecule, with a given torque $\tau = k_B T$ acting upon its free end, is obtained by performing in the r.h.s. of the recurrence relation (27) the following replacement:

$T_{WLC}(n+1; n; f) \rightarrow T_{RLC}(n+1; n; f; \tau^2)$, where T_{RLC} is given explicitly in ref.[11]. The anchoring-plate barrier is expected to have significant effects upon the so-called "hat curves", giving, for a fixed force, the relative elongation versus the supercoiling reduced parameter τ . Let us take the "low" force case, $F \approx 0.1 \text{ pN}$, where the RLC model "hat curve" dips steeply into the negative z region when $j \approx 0.03$. This effect is attributed to the creation of plectonem structures which are allowed to wander in the $z < 0$ half plane, because of the vanishing of their stretching-potential energy. Therefore, we can expect important modifications once the spatial constraints, which forbid the $z < 0$ region, are incorporated.

APPENDIX A: TRANSFER MATRIX VERSUS HAMILTONIAN METHODS FOR DS-DNA SUBJECT TO SPATIAL CONSTRAINTS.

1. The auxiliary variable method.

Our starting point, as in section I, is the following partition function:

$$Z = \int_0^L D[r] \exp \int_0^L E(s) ds; \quad (A1)$$

$$E(s) = E_0(\underline{r}^2) + \frac{1}{2} A \dot{r}^2 - \underline{f} \cdot \underline{r} + V(r); \quad (A2)$$

with $\underline{r} = \frac{d\mathbf{r}}{ds}$ and $r = \frac{d^2}{ds^2}(\mathbf{r})$. The variable s with $0 \leq s \leq L$ results from a coarse graining of the molecular chain. We have seen that, for a suitable choice of $E_0(\underline{r}^2)$, the variable s coincides, to an arbitrary precision, with the arc-length s of a rectifiable curve.

To compute the partition function, the first step involves the discretization of the variable s : $s_n = n \cdot b$. The molecular chain is then represented by N elementary links or effective monomers with $N = L/b$. Assuming that the effective monomer length b is much smaller than the persistence length A , we replace the derivative by finite differences:

$$\underline{r} = \frac{\mathbf{r}_n - \mathbf{r}_{n-1}}{b}; \quad r = \frac{\mathbf{r}_n - 2\mathbf{r}_{n-1} + \mathbf{r}_{n-2}}{b^2}; \quad (A3)$$

The partition function is then written as a multiple integral of a product of $N - 1$ functions of the monomer-coordinates r_n :

$$Z = \int \prod_{n=1}^{N-1} dr_n \int \prod_{n=2}^N du_n \exp(-bE_{\text{disc}}(n)) g Z_{\text{in}}(r_1; r_0): \quad (\text{A } 4)$$

We are going to use a standard field-theory trick to eliminate high order derivatives without having to plug by hand Dirac delta functions into the functional integral. This involves the introduction of an auxiliary dynamical variable u . The starting point is the integral identity, written for fixed n :

$$\exp\left(-\frac{bA}{2}(r_n)^2\right) g C(A)^{-1} \int du_n \exp\left(-\frac{bA}{2}(u_n + ir_n)^2 + r_n^2\right) g; \quad (\text{A } 5)$$

where $C(A) = \int du_n \exp\left(-\frac{b}{2A}(u_n + iAr_n)^2\right) g = \left(\frac{2A}{b}\right)^{\frac{1}{2}}$: Expanding the argument of the exponential we get the final identity:

$$\exp\left(-\frac{bA}{2}(r_n)^2\right) g C(A)^{-1} \int du_n \exp\left(-b\frac{1}{2A}u_n^2 + iu_n r_n\right) g: \quad (\text{A } 6)$$

Ignoring the overall factor $C(A)^{-N}$, we arrive in this way to an expression of $E(s)$ involving, now, the two variables r and u :

$$E(s) = E_0(r)^2 + iA \int dr u \cdot r + \frac{1}{2A} \int dr u^2 - \int dr V(r): \quad (\text{A } 7)$$

We perform the following integration by part:

$$\int_0^L du \cdot r = \left[u \cdot r \right]_0^L - \int_0^L ds (r \cdot u): \quad (\text{A } 8)$$

Ignoring the "surface term", which can be estimated to be of the order of $1/N$, we obtain the new expression of the elastic-energy density:

$$E^{\text{new}}(s) = E_0(r^2) - i \int dr r \cdot \left(\frac{1}{2A} u^2 + V(r) \right): \quad (\text{A } 9)$$

We have now a "kinetic term", which depends only upon first-order derivatives, so that the construction of the quantum Hamiltonian from the functional integral is now a relatively straightforward affair. However, a price has to be paid: some extra-work will be required to elucidate the physical meaning of the auxiliary dynamical variable u . We must now write the discrete version of $E^{\text{new}}(s)$. Using the same kind of prescription as in Section I, one gets easily:

$$E_{\text{disc}}^{\text{new}}(n) = E_0\left(\frac{(r_n - r_{n-1})^2}{b^2}\right) - \frac{i}{b^2}(r_n - r_{n-1}) \cdot (u_n - u_{n-1}) + V(r_n) + \frac{1}{2A} u_n^2: \quad (\text{A } 10)$$

We have omitted the constant force f contribution since it can be easily added up at the end. We note that the "kinetic term"

$$K_0(r_n - r_{n-1}; u_n - u_{n-1}) = E_0\left(\frac{(r_n - r_{n-1})^2}{b^2}\right) - \frac{i}{b^2}(r_n - r_{n-1}) \cdot (u_n - u_{n-1}); \quad (\text{A } 11)$$

is symmetric under the exchanges: $r_n \leftrightarrow r_{n-1}$; $u_n \leftrightarrow u_{n-1}$, while the "potential" contribution $U(r_n; u_n) = V(r_n) + \frac{1}{2A} u_n^2$ is clearly not. We can make $E_{\text{disc}}^{\text{new}}(n)$ symmetric by simply doing the replacement $U(r_n; u_n) \rightarrow (U(r_n; u_n) + U(r_n; u_{n-1}))/2$. We not only remain within the leeway involved in any discretization procedure, but we also obtain an improvement since a trapezoidal integration is better than a rectangular one.

The transfer matrix associated with the symmetrized energy density $E_{\text{disc}}^{\text{new}}(n+1)$ reads as follows:

$$\begin{aligned} T^{\text{new}}(r_{n+1}; u_{n+1} | r_n; u_n) &= \exp(-bE_{\text{disc}}^{\text{new}}(n+1)) \\ &= \exp(-b[K_0(r_{n+1} - r_n; u_{n+1} - u_n) + U(r_{n+1}; u_{n+1}) + U(r_n; u_n)]/2): \end{aligned} \quad (\text{A } 12)$$

We define the transfer operator \mathcal{T}^{new} associated with the transfer matrix by writing:

$$\langle r_{n+1}; u_{n+1} | \mathcal{T}^{\text{new}} | r_n; u_n \rangle = T^{\text{new}}(r_{n+1}; u_{n+1} | r_n; u_n): \quad (\text{A } 13)$$

In the following, $\hat{\mathcal{P}}$ will stand for linear operators acting upon functions $f(r_n; u_n)$ of the dynamical variables. If $f(r_n; u_n)$ is an eigenfunction, then the associated eigenvalue will be written without hat: X .

Let us isolate the "kinetic" part of $\hat{\mathcal{P}}^{\text{new}}$ by writing:

$$\hat{\mathcal{P}}^{\text{new}} = \exp \left(\frac{b}{2} \hat{\mathcal{P}} \right) \hat{\mathcal{T}}_0^{\text{new}} \exp \left(\frac{b}{2} \hat{\mathcal{P}} \right); \quad (\text{A } 14)$$

$$\langle r_{n+1}; u_{n+1} | \hat{\mathcal{T}}_0^{\text{new}} | r_n; u_n \rangle = \exp \left(-b K_0(r_{n+1} - r_n; u_{n+1} - u_n) \right); \quad (\text{A } 15)$$

where $\hat{\mathcal{P}}$ is the operator associated with the potential $U(r_n; u_n)$ and $K_0(r_{n+1} - r_n; u_{n+1} - u_n)$ the "kinetic" elastic-density term given by eq.(A 11). We note that the "kinetic" transfer operator $\hat{\mathcal{T}}_0^{\text{new}}$ is invariant upon space translations: $r \rightarrow r+a$ and $u \rightarrow u+b$. This implies that $\hat{\mathcal{T}}_0^{\text{new}}$ is diagonal within the momentum basis defined by $\langle r | \hat{p}_r \rangle = \exp i p_r r$ and $\langle u | \hat{p}_u \rangle = \exp i p_u u$. Performing the involved Fourier transforms, we get readily the matrix element of $\hat{\mathcal{T}}_0^{\text{new}}$ in the momentum basis:

$$\begin{aligned} \langle p_{r_{n+1}}; p_{u_{n+1}} | \hat{\mathcal{T}}_0^{\text{new}} | p_{r_n}; p_{u_n} \rangle &= (2\pi)^{-3} \langle p_{r_{n+1}} - p_{r_n} \rangle^3 \langle p_{u_{n+1}} - p_{u_n} \rangle \hat{\mathcal{T}}_0^{\text{new}}(p_{r_n}; p_{u_n}); \\ \hat{\mathcal{T}}_0^{\text{new}}(p_{r_n}; p_{u_n}) &= (2\pi)^{-3} \exp \left\{ -b E_0(p_{u_n}^2) + i p_{u_n} p_{r_n} g \right\}; \end{aligned} \quad (\text{A } 16)$$

The two δ -functions appearing above reflect the translation invariance of the transfer operator $\hat{\mathcal{T}}_0$. We note that p_{u_n} has taken the place of the velocity $v_n = \dot{r}_n$ in $E_0(\dot{r}_n^2)$. This suggests that p_u can be identified with the velocity v , as we are going to prove later on. We have now all what we need to write $\hat{\mathcal{T}}_0$ as the exponential of an Hamiltonian operator $\hat{\mathcal{H}}_0$ symmetric in Fourier space, but non-Hermitian. Returning to the ordinary space, we introduce the conjugate momentum operators relative to the dynamical variables r and u :

$$\hat{p}_r = -i r; \hat{p}_u = -i u; \quad (\text{A } 17)$$

Let us remind that the transformation $f(p_r) \rightarrow p_r f(p_r)$, written in the Fourier space, reads in ordinary space $f(r) \rightarrow \hat{p}_r f(r)$ (similarly for the variable u); so we can write $\hat{\mathcal{T}}_0^{\text{new}}$ as the differential operator $\exp(-b \hat{\mathcal{H}}_0^{\text{new}})$, where $\hat{\mathcal{H}}_0^{\text{new}}$ is given, up to an irrelevant additive constant, by the following expression:

$$\hat{\mathcal{H}}_0^{\text{new}} = E_0(\hat{p}_u^2) + i \hat{p}_u \hat{p}_r; \quad (\text{A } 18)$$

The transfer operator $\hat{\mathcal{T}}^{\text{new}}$, defined in eq.(A 14), reads then as follows:

$$\hat{\mathcal{T}}^{\text{new}} = \exp \left(\frac{b}{2} \hat{\mathcal{P}} \right) \exp \left(-b \hat{\mathcal{H}}_0^{\text{new}} \right) \exp \left(\frac{b}{2} \hat{\mathcal{P}} \right); \quad (\text{A } 19)$$

Using the Campbell-Hausdorff formula one can derive the following expression for $\hat{\mathcal{T}}^{\text{new}}$ [25]:

$$\hat{\mathcal{T}}^{\text{new}} = \exp \left\{ -b \hat{\mathcal{H}}_0^{\text{new}} + \frac{b^2}{24} (2 [\hat{\mathcal{P}}; \hat{\mathcal{H}}_0^{\text{new}}]; \hat{\mathcal{P}}] - [\hat{\mathcal{P}}; \hat{\mathcal{H}}_0^{\text{new}}]; \hat{\mathcal{H}}_0^{\text{new}} \right\} + O(b^3); \quad (\text{A } 20)$$

The total Hamiltonian $\hat{\mathcal{H}}_{\text{new}}$ is readily obtained as the lowest order term with respect to b :

$$\hat{\mathcal{H}}^{\text{new}} = \hat{\mathcal{H}}_0^{\text{new}} + \hat{\mathcal{P}} = E_0(\hat{p}_u^2) + i \hat{p}_u \hat{p}_r + V(r) + \frac{1}{2A} u^2; \quad (\text{A } 21)$$

Another interest of the above formula is to allow a comparison of the symmetric transfer operator $\hat{\mathcal{T}}^{\text{new}}$ connecting adjacent effective monomers along the discretized chain with the exact evolution operator $\exp(-b \hat{\mathcal{H}}^{\text{new}})$ associated with a jump $s = b$ along the original continuous chain. The formula (A 20) shows clearly that the absolute uncertainty introduced by using $\hat{\mathcal{T}}^{\text{new}}$ instead of the exact evolution operator is of the order of b^3 . The use of an unsymmetrized transfer matrix would have led to an absolute uncertainty of the order b^2 .

2. Physical interpretation of the auxiliary variable u : the normal form of the Hamiltonian.

In the above derivation of $\hat{\mathcal{H}}^{\text{new}}$, the auxiliary variable u and its conjugate momentum operator \hat{p}_u have been introduced in a rather formal way. We would like to show that the operator \hat{p}_u has a well defined physical interpretation. The fact that it replaces \dot{r} in going from E_{new} to $\hat{\mathcal{H}}$, suggests that these two quantities are identical.

To get an explicit proof, it is convenient to introduce the "Euclidian Heisenberg" operator relative to the monomer coordinate along the chain:

$$\hat{r}(s) = \exp(s\hat{H}) r \exp(-s\hat{H}) \quad (\text{A } 22)$$

These operators enter in the computation of the correlation function of the two-monomer coordinates which is given by the standard formula [23]:

$$C(r_i(s_1); r_j(s_2)) = \text{Tr}(\exp(-L\hat{H}) \hat{r}_i(s_1) \hat{r}_j(s_2)) = \text{Tr} \exp(-L\hat{H}) : \quad (\text{A } 23)$$

The two-monomer correlation function relative to the velocities is obtained by taking the partial derivatives of $C(r_i(s_1); r_j(s_2))$ with respect to s_1 and s_2 . We have then to compute the s -derivative of $\hat{r}(s)$:

$$\dot{r}(s) = \frac{d\hat{r}(s)}{ds} = \exp(s\hat{H}) [\hat{H}; r] \exp(-s\hat{H}) = \hat{p}_u(s) \quad (\text{A } 24)$$

Going to the limit $s \rightarrow 0$ the operator \hat{p}_u is just the Euclidian velocity operator $\hat{v} = [\hat{H}; r]$. It is clear that the above computation can be applied to more general situations where $\hat{r}_j(s_2)$ is replaced by any physical operator. Let us choose, for instance, the Unit operator \mathbb{I} . One obtains readily a simple physical confirmation of the \hat{p}_u , \dot{r} identity through the following relations between their averages:

$$\langle \dot{r}(s) \rangle = \langle v(s) \rangle = \langle p_u(s) \rangle \quad (\text{A } 25)$$

In all the explicit computations to be performed later on, we shall use a functional basis diagonal with respect to the velocity vector operator $\hat{v} = v$, where the real vector v stands for the three corresponding eigenvalues. We can use a more familiar language by working with the Fourier transforms of the wave functions: $\langle u | = \int d^3v \exp(iu \cdot v) \langle v |$. The two linear transformations $\langle u | \rightarrow \hat{p}_u \langle u |$ and $\langle u | \rightarrow u \langle u |$ read respectively in Fourier space: $\langle v | \rightarrow v \langle v |$ and $\langle v | \rightarrow i r_v \langle v |$. We get the final expression for the "physical" Hamiltonian \hat{H} by performing upon \hat{H}^{new} the replacement $\hat{p}_u \rightarrow \hat{v}$ and $u \rightarrow i r_v$:

$$\hat{H} = \frac{1}{2A} r_v^2 + E_0(v^2) + v \cdot (f - f) + V(r) \quad (\text{A } 26)$$

As noted before, \hat{H} is not an Hermitian operator, but if $V(r)$ is an even function of r , it is self-adjoint with respect to the functional scalar product: $\langle \cdot | \cdot \rangle = \int d^3v d^3r \langle \cdot | (v; r) \rangle \langle \cdot | (v; r)$.

3. The Spatially Constrained WLC Hamiltonian.

In order to apply the present formalism to the WLC model with spatial constraints, we have to take an adequate functional form for $E_0(v^2)$. As it was shown previously in section I, the solution is rather simple: one introduces the small length b such that $b \ll 1$ and one chooses for $E_0(v^2)$ the following expression:

$$E_0(v^2) = b \frac{(v^2 - 1)^2}{2 b^2} \quad (\text{A } 27)$$

Introducing the above choice of $E_0(v^2)$ in the final expression for the Hamiltonian \hat{H} given by equation (A 26), we get the Hamiltonian $\hat{H}(b)$:

$$\hat{H}(b) = \frac{1}{2A} r_v^2 + b \frac{(v^2 - 1)^2}{2 b^2} + v \cdot (f - f) + V(r) \quad (\text{A } 28)$$

Performing the trace upon $v = |v|$ upon the transfer operator $\exp(-b\hat{H}(v; b))$, only the value $v = 1$ does contribute in the limit $b \rightarrow 0$, so that v coincides with the unitary tangent vector t appearing in the WLC model. We arrive in this way to the WLC Hamiltonian adequate for spatially constrained dsDNA [12, 13, 14, 15, 16, 17, 18, 19, 20, 21, 22]:

$$\hat{H}_{\text{SCWLC}} = \frac{1}{2A} r_t^2 - f \cdot t + t \cdot r \cdot V(r) = \hat{H}_{\text{WLC}}(f) + t \cdot r + V(r) \quad (\text{A } 29)$$

If $V(r) = 0$, it is easily seen that \hat{H}_{SCWLC} is diagonal in the momentum space. Performing the trace with respect to r upon the exact transfer matrix is equivalent, within the momentum basis, to take the limit $p_r \rightarrow 0$. In this way, the standard WLC model Hamiltonian is immediately recovered [20].

4. The transfer matrix deduced from the SCWLC Hamiltonian.

It is of interest to compare the symmetric transfer matrix obtained from the Hamiltonian \hat{H}_{SCWLC} , by an equation similar to (A19), to the one derived in Section I, directly from the the partition functional integral of eq.(15).

To proceed, we write the Hamiltonian \hat{H}_{SCWLC} of eq.(A29) under the following compact form :

$$\hat{H}_{SCWLC} = \hat{H}_{WLC}(f, \hat{p}_r) + V(r) : \quad (A30)$$

Using eq.(A20), the exact transfer operator $\exp(-\hat{H}_{SCWLC})$ can be written, up to corrections of the order of b^3 , as follows :

$$\hat{T}_{SCWLC} = \exp\left[-\frac{b}{2} \int \hat{p}^2 dr\right] \exp\left[-b \hat{H}_{WLC}(f, \hat{p}_r)\right] \exp\left[-\frac{b}{2} \int V(r) dr\right] : \quad (A31)$$

We can write the recurrence relation obeyed by the partition function $Z_n(r_n; t_n)$ using the transfer matrix associated with \hat{T}_{SCWLC} :

$$Z_{n+1}(r_{n+1}; t_{n+1}) = \int dr_n \int dt_n \exp\left[-\frac{b}{2} \int V(r) dr\right] \hat{T}_{WLC}(f, \hat{p}_r) Z_n(r_n; t_n) : \quad (A32)$$

Let us, first, evaluate the matrix element of $\hat{T}_{WLC}(f, \hat{p}_r)$, which is diagonal in the momentum basis. The corresponding diagonal element is just the WLC model transfer matrix given in equation (25) for the case of a complex force $f = ip_r$. We get in this way an intermediate expression of the $\hat{T}_{WLC}(f, \hat{p}_r)$ matrix element, within the coordinate space, written as a Fourier integral:

$$\langle r_{n+1}; t_{n+1} | \hat{T}_{WLC}(f, \hat{p}_r) | r_n; t_n \rangle = \int \frac{d^3 p_r}{(2\pi)^3} \exp[ip_r \cdot r_n - r_{n+1} + b \frac{t_{n+1} + t_n}{2}] \langle r_{n+1}; t_{n+1} | \hat{T}_{WLC}(f) | r_n; t_n \rangle : \quad (A33)$$

The integration over p_r gives a Dirac δ -function which is similar to that introduced by hand in Section I:

$$\langle r_{n+1}; t_{n+1} | \hat{T}_{WLC}(f, \hat{p}_r) | r_n; t_n \rangle = \int dr_n \int dt_n \delta(r_{n+1} - r_n - b \frac{t_{n+1} + t_n}{2}) \langle r_{n+1}; t_{n+1} | \hat{T}_{WLC}(f) | r_n; t_n \rangle : \quad (A34)$$

Performing the integration over r_n leads immediately to the partition-function recurrence relation:

$$Z_{n+1}(r_{n+1}; t_{n+1}) = \exp\left[-\frac{b}{2} V(r_{n+1})\right] \int dt_n \exp\left[-\frac{b}{2} V(r_{n+1}) - \frac{b}{2} (t_{n+1} + t_n) g\right] \langle r_{n+1}; t_{n+1} | \hat{T}_{WLC}(f) | r_{n+1} - \frac{b}{2} (t_{n+1} + t_n); t_n \rangle : \quad (A35)$$

5. Relation between the symmetric and asymmetric transfer matrices.

In principle, one can build a numerical iteration procedure from the above recurrence relation. It will turn out to be more complex and physically less transparent than the one which is actually used in the present paper. We are going to describe the simplifications to be made on eq.(A35) in order to recover the recurrence relation (26) derived directly in Section I, by starting from the Boltzmann functional integral.

a. Basic assumptions. In order to justify this procedure, we shall assume that the rates of variation with r, t , both of the potential $V(r)$ and the starting partition function $Z_0(r; t)$, are at most of the order of the inverse of the persistence length A , which is assumed to be at least ten times larger than the length b of the elementary link. More precisely we shall impose the two constraints: $Z_0(r; t)^{-1} r_r Z_0(r; t) \leq A^{-1}$ and $V(r)^{-1} r_r V(r) \leq A^{-1}$. In the computations presented in Section II, these constraints were indeed satisfied. One can prove by recurrence that these estimates hold also for $Z_n(r_n; t_n)$. This last point can be verified by looking at the the probability distributions $P(z; L)$ plotted on Fig. 5, where A is taken as the length unit. This will allow us to make two important simplifications:

b. Simplification 1. The two Boltzmann factors involving the potential $V(r)$ can be replaced by a single one, namely: $\exp(-bV(r_{n+1}))$: For the confining potential $V(z)$ used in this paper, we have found that the corresponding Boltzmann factor corrections are about 2% ; they are localized near the two plate barriers in narrow regions of width A . Their overall effect is expected to be somewhat smaller, since the width of the potential well is $> 20A$.

c. Simplification 2. The second simplification is a change of the monomer coordinate in the partition function Z_n appearing in the r.h.s of eq.(A 35):

$r_{n+1}^b = r_{n+1} - \frac{b}{2}(t_{n+1} + t_n)$; $r_{n+1}^a = r_{n+1} - bt_{n+1}$: It is to convenient rewrite r_{n+1}^a and r_{n+1}^b in terms of $t_n = (t_{n+1} - t_n)$:

$$r_{n+1}^a = r_{n+1} - bt_n - bt_{n+1} \quad \text{and} \quad r_{n+1}^b = r_{n+1} - bt_n - b=2 t_n : \quad (\text{A } 36)$$

We get expressions for the probability distributions $P^a(r_{n+1})$ (in the limit $b \rightarrow 0$) by integration over t_{n+1} of the two sides of eq.(26) and then exchange of the integration order:

$$P^a(r_{n+1}) = \int \int \exp(-bV(r_{n+1})) \frac{d^2(t_n)}{Z} \frac{d^2(t_{n+1})}{Z} \exp\left(\frac{b}{2A} t_n^2\right) Z_n(r_{n+1} - bt_n - bt_{n+1}; t_n):$$

We now make a first order Taylor expansion of Z_n with respect to bt_n and perform the Gaussian average over t_n using t_{n+1} as integration variable. We arrive in this way to a formula useful for our purpose:

$$P^a(r_{n+1}) = \exp(-bV(r_{n+1})) \int \frac{d^2(t_n)}{Z} \left(1 - \frac{b^2}{A} r_{n+1} t_n\right) Z_n(r_{n+1} - bt_n; t_n): \quad (\text{A } 37)$$

The formula for $P^b(r_{n+1})$ is obtained by multiplying by $b=2$ the $b^2=A$ term, as it follows immediately from eq.(A 36.) Using the above basic assumptions, one finds that the difference $P^a(r_{n+1}) - P^b(r_{n+1})$ is $\frac{1}{2}(b=A)^2$ and this reflects the lack of symmetry of the transfer matrix used in Section I. By implementing the simplifications 1. and 2. in equation (A 35), we recover immediately the partition function recurrence relation derived in Section I (eq.(26):

$$Z_{n+1}(r_{n+1}; t_{n+1}) = \exp(-bV(r_{n+1})) \int \frac{d^3 t_n}{Z} \exp\left(\frac{b}{2A} t_n^2\right) \int \frac{d^2 t_{n+1}}{Z} \exp\left(\frac{b}{2A} t_{n+1}^2\right) Z_n(r_{n+1} - bt_{n+1}; t_n): \quad (\text{A } 38)$$

ACKNOWLEDGMENTS

It is a pleasure to thank D. Bensimon, M.-A. Bouchiat and J. Ilipoulos for their careful reading of this manuscript and valuable suggestions.

Laboratoire de Physique Theorique de l'Ecole Normale Supérieure is a Unité Mixte du Centre National de la Recherche Scientifique et de l'Ecole Normale Supérieure (UMR 8549).

-
- [1] C. Bustamante, Z. Bryant and S. Smith, Nature 421, 423-427 (2003).
 - [2] J.F. Allemand, D. Bensimon and V. Croquette, Curr. Op. Structural Biology 13, 266-274 (2003).
 - [3] S.B. Smith, L. Finzi and C. Bustamante, Science 258, 1122 (1992).
 - [4] T.T. Perkins, S.R. Quake, D.E. Smith and S. Chu, Science 264, 8222 (1994).
 - [5] T.R. Strick, J.-F. Allemand, D. Bensimon, A. Bensimon and V. Croquette, Science 271, 1835 (1996).
 - [6] M. Fixman and J. Kovac, J. Chem. Phys. 58, 1564 (1973).
 - [7] J.F. Marko and E.D. Siggia, Science 265, 506 (1994).
 - [8] C. Bouchiat, M.D. Wang, S.M. Block, J.-F. Allemand and V. Croquette, Biophys. J. 76, 409 (1999).
 - [9] J.D. Meroz and P. Nelson, Proc. Natl. Acad. Sci. USA 94, 11418 (1997), Macromolecules 3, 6333 (1998).
 - [10] C. Bouchiat and M. Mezard, Phys. Rev. Lett. 80, 1556 (1998).
 - [11] C. Bouchiat and M. Mezard, Eur. Phys. J. E. 2, 377-402 (2000).
 - [12] A.C. Maggs, D.A. Huse and S. Leibler Europhys. Lett. 8, 615 (1988).
 - [13] G. Gompper and T.W. Burkhardt, Phys. Rev. A , 6124 (1989).
 - [14] T.W. Burkhardt, J. Phys A 26, L1157-L1162 (1993).
 - [15] T.W. Burkhardt, J. Phys A 30, L167-L172 (1997).
 - [16] D. J. Bicout and J.T. W. Burkhardt, J. Phys. A 34, 5745 (2001).

- [17] J. Kierfeld and R. Lipowsky, J. Phys. A 38 L155-L161 (2005).
- [18] N. Saito, K. Takahashi and Y. Yunoki, J. Phys. Soc. Japan, 22, 219-236 (1967)
- [19] Karl L. Fried, J. Chem. Phys. 44, 1153-1463 (1971).
- [20] H. Yamakawa, in Helical Worm like Chains in Polymer Solutions (Springer-Verlag, New-York, 1997), chapter 3, 19-47.
- [21] E. Helfand and Y. Tagami, J. Chem. Phys. 56, 3592-3601, (1971)
- [22] D. C. Morse and G. H. Fredrickson, Phys. Rev. Lett. 73, 3235 (1994).
- [23] G. Parisi, in Statistical Field Theory in Advanced Book Classics, (Perseus Books 1998).
- [24] The transfer matrix method was applied to the solution of the one- and two-dimensional Ising Models, by K. Huang in Statistical Mechanics, (John Wiley and Sons, New York, 1988). A good pedagogical introduction to the formalism used in the present paper is found in reference [23]. The authors of reference [17], working within a continuous formalism, call transfer matrices mathematical objects which are usually known under the name of Green functions: see equations (3) and (7).
- [25] J. Iliopoulos, Private communication.
- [26] A. Cnut, D. Lasne, J.-F. Allen and, M. Dahan and P. Desbieres, Phys. Rev. E 67, 051910 (2003)
- [27] A. Revyakin, R. H. Ebright, and T. R. Strick, Nature Methods, 2, 127-138 (2005)